Sawcut Depth Considerations for Jointed Concrete Pavement Based on Fracture Mechanics Analysis

DAN G. ZOLLINGER, TIANXI TANG, AND DAPENG XIN

The efficient control of slab cracking that develops in concrete pavements is important to pavement performance. From the viewpoint of engineering analysis and the design of pavements it is desirable to control pavement cracking to joint locations at desirable intervals to decrease the possibility of uncontrolled cracking. An approach for estimating appropriate sawcut depths and placement timing by using fracture mechanics for jointed concrete systems is suggested. Early-age sawcutting, as one form of crack induction, has been applied to concrete pavement surfaces at specific contraction joint locations. A mechanics-based approach to the determination of sawcut depth and spacing requirements by fracture mechanics analysis is presented. The stress field in a concrete slab induced by thermal and shrinkage gradients is based on curling and warping analysis, which also leads to sawcut spacing criteria. The fracture parameters K_{If} and C_f defined by the size effect law are obtained from laboratory notched beam fracture tests for specific coarse aggregate types. Modified linear elastic fracture mechanics is applied to determine a sufficient notch or sawcut depth to ensure controlled cracking. Preliminary field results show that early-age sawcutting with appropriately determined joint spacing and depth can be used for the positive control of cracking in jointed plain concrete pavements. The theoretical sawcut depth, as determined by fracture analysis, that can be used in pavement construction practice, is significantly less than the conventional $d/3$ or $d/4$, where d is the slab thickness. Recent pavement surveys have verified this conclusion.

In newly paved concrete pavements the temperature rise caused by the hydration process can be considerable. If unrestrained the concrete pavement can expand and contract during the heating and subsequent cooling process without stresses being induced. Similar displacements may result because of shrinkage as the pavement dries and expands when it is wetted. However, actual pavements in the field are nearly always restrained to some degree by either an external restraint such as friction, the slab weight, tied adjoining lanes, or a combination of these. The interaction of the induced temperature and drying shrinkage gradients and the slab restraint can induce tensile stresses that lead to slab cracking. Field experiments have indicated that many sawcut joints in the concrete pavement typically break within the first few days after placement when concrete is poured under hot weather conditions. It is evident that an understanding of the mechanism related to early-age cracking in concrete pavements should provide a basis for making improvements in current pavement sawcutting practices with respect to an appropriate combination of sawcut timing and sawcut depths. The sawcut should be deep enough such that a crack initiated at a sawcut surface notch will propagate in an unstable manner from the sawcut tip to the slab bottom under stresses caused by temperature and shrinkage gradients or variations. Since this cracking consumes the elastic energy that developed within the concrete slab, stress and the incidence of cracking elsewhere are reduced in the slab. The controlled cracks reduce the restraint in the concrete pavement slab and therefore lower the maximum tensile stress. Since the early 1950s one-third of the pavement thickness ($d/3$) has been accepted and assumed to be the necessary depth of cut to induce cracking. However, literature reviews reveal little technical justification for this assumption other than field experience in isolated instances of uncontrolled cracking in which engineers may have assumed that deeper sawcuts would solve the problems with random cracking that they were experiencing. It will be shown later that the depth of the sawcut is dependent on the fracture strength of the concrete and that the most significant factor in the effective control of random cracking is the time of sawcut placement. In this sense the use of a sawcut depth of $d/3$ or $d/4$ in all instances without respect to aggregate type, concrete properties, or pavement thickness characteristics is technically unjustified. The conventional analysis of crack development in sawcut concrete pavement typically assumes a flawless beam or plate, although crack formation and development are of primary interest. In this paper fracture mechanics is applied to determine sawcut depth requirements on the basis of the stresses that develop during the first few days after concrete placement. Since the use of fracture mechanics to analyze sawcut depth criteria in jointed concrete systems constitutes a new approach to the analysis of crack development (and basically a rational approach to accurately account for the factors pointed out above), sufficient mathematical derivation will be provided to adequately document and justify the approach.

Texas Transportation Institute, Texas A&M University, College Station, Tex. 77843-3135.

THEORETICAL APPROACH: CLIMATIC STRESSES

Environmental stresses in concrete pavements can be attributed to both temperature and drying shrinkage effects and are particularly important at an early age. Stresses caused by both of these effects are discussed subsequently.

Thermal Stresses

Because of exposure to ambient conditions a concrete pavement may cool to a minimum temperature after cycling through a maximum temperature such that tensile stresses can be induced in the slab. The tensile stress distribution through the pavement thick-

ness can be assumed to be linear for the sake of simplicity, but others (*1,2*) have indicated that the distribution may be decomposed into three parts: axial stress, curling stress, and nonlinear stress. The stress distribution is caused not only by a temperature effect but may also be caused by moisture effects. Therefore, a complete analysis of early-age stresses will include curling, warping, and frictional stresses in which the axial stress component may be primarily due to subbase/subgrade frictional effects. Stress development may become significant very soon after placement, perhaps even before the concrete has attained a certain degree of stiffness (which may not occur until 18 to 24 hr after placement) has developed. Crack development in concrete pavements has been noted to be sensitive to diurnal temperature effects. The tendency to curl is restrained by the slab weight, in which the resulting level of stress development is a function of the stiffness of the subbase layer as reflected in the radius of relative stiffness (*l*). When the slab curls in an upward configuration, tensile stresses are induced in the upper part of the slab, whereas compressive stresses are induced in the lower part. Analysis of induced stresses by a linear temperature gradient in rigid pavements was developed by Westergaard (*3*) and others (*4*).

The Westergaard solution for slab stresses under temperature gradients will not be elaborated here. However, a similar approach for slab stresses caused by moisture gradients will be presented later. Westergaard presented solutions that considered curling stresses in a slab of infinite and semi-infinite dimensions on the basis of the following governing equations:

$$l^4 \frac{d^4w}{dy^4} + kw = 0 \tag{1}$$

where

$$l = \left[\frac{Eh^3}{12(1 - \nu^2)k}\right]^{1/4}$$

E = Young's modulus (psi),
ν = Poisson's ratio,
k = foundation modulus (psi/in.),
h = slab thickness (in.), and
w = slab deflection (in.).

Equation 1 encompasses a spring model that was proposed for the base reaction with the k value as the spring modulus. Although the slab weight restrains the curling, the weight is not included in the equation. However, the displacement (w) caused by curling can be considered only part of the slab displacement (*5*). In addition to w, the slab weight causes a uniform subsidence (w_s). The total displacement w_t is the sum of w_s and w. So long as $w_t = w_s + w \geq 0$, the spring model is valid even if $w < 0$.

The solution to Equation 1 indicates a negative w or upward displacements at or near the slab edge in concave curling, which should not be interpreted that the slab is pulled down there by the base (i.e., the Winkler spring should be released). Whenever w is less than 0, part of the slab weight is supported by the base, whereas the rest of it is supported by the slab itself, which contributes to the stresses in the slab. The total displacement w_t must be positive, otherwise Equation 1 is not valid. Further explanation is provided elsewhere (*5*).

Nonetheless, from Westergaard's analysis the maximum curling stress (σ_0) far away from the slab edge boundary is

$$\sigma_0 = \sigma' = \frac{E_c \alpha t}{2(1 - \nu)} = \frac{E_c}{2(1 - \nu)} \epsilon' \tag{2}$$

where

α = thermal coefficient of expansion (/°F),
t = temperature change or drop, and
$\epsilon' = \alpha t$.

Bradbury (*4*) developed coefficients on the basis of the Westergaard solution as applied to slabs of practical dimensions. The coefficients are used in the following equations:

Edge stress:

$$\sigma = \frac{CE_c\alpha t}{2} = C(1 - \nu)\,\sigma' \tag{3}$$

Interior stress:

$$\sigma = \frac{E_c\alpha t}{2}\left(\frac{C_1 + \nu C_2}{1 - \nu^2}\right) = \left(\frac{C_1 + \nu\, C_2}{1 - \nu^2}\right)\sigma'(1 - \nu)$$

$$= \sigma'\left(\frac{C_1 + \nu C_2}{1 + \nu}\right) \tag{4}$$

If $C_1 = C_2 = C$, then $\sigma = C\sigma'$.

The coefficient C_1 is the desired direction, whereas C_2 is for the direction perpendicular to this direction. L_x and L_y are the free length and width, respectively.

Shrinkage Stresses

Similarly, the interaction of drying shrinkage (ϵ^{sh}) of concrete and pavement restraint can induce stresses in a concrete slab. According to Bažant and Wu (*6*), the shrinkage of concrete can be described by the following function of humidity:

$$\epsilon^{sh} = \epsilon^{sh\infty}\,(1 - h^3)\ \text{(microstrain)} \tag{5}$$

where h (or rh to avoid confusion with slab thickness) in this and following expressions is the relative humidity, and $\epsilon^{sh\infty}$ is a material parameter, which is the ultimate concrete shrinkage at the reference rh of 50 percent. A formula from the model of Bažant and Panula (*7*) for calculating $\epsilon^{sh\infty}$ is applied here:

$$\epsilon^{sh\infty} = 1{,}330 - 970y \tag{6}$$

$$y = (390z^{-4} + 1)^{-1} \tag{7}$$

$$z = 0.381\sqrt{f'_{28}}\left[1.25\left(\frac{a}{c}\right)^{1/2} + 0.5\left(\frac{g}{s}\right)^2\right]^{1/3}\left(\frac{1 + \frac{s}{c}}{\frac{w}{c}}\right) - 12 \tag{8}$$

where

a/c = total aggregate/cement ratio,
g/s = coarse aggregate/fine aggregate ratio,
s/c = fine aggregate/cement ratio,
w/c = water/cement ratio, and
f'_{28} = 28-day cylinder compressive strength (psi).

In the middle portion of an infinitely large concrete slab where $(\partial^2w/\partial x^2) = (\partial^2w/\partial y^2) = 0$, the curling or warping strain is totally

restrained. Therefore, the shrinkage-induced stress at this location (σ^{sh}) is

$$\sigma_x = \sigma_y = \frac{E_c}{1 - \nu} \epsilon^{sh} \tag{9}$$

Moisture measurements in actual field slabs obtained by using instrumentation described by others (*8*) have indicated that the drying process tends to occur to some extent vertically through the slab. These measurements have also indicated the nonlinearity of the humidity profile vertically through a pavement slab during wetting and drying cycles. One would expect that such variations would result in similar profiles or distributions of moisture-induced warping stresses. The representation of these distributions numerically in an analysis may well require sophisticated methods such as the finite-element or finite-difference approaches. However, for the purpose of introducing an approach to the analysis of moisture-induced warping, the moisture-induced stress distribution in a concrete slab is simplified (as was done for temperature gradient-related stresses) to vary linearly along the thickness with the maximum tensile stress σ^{sh} at the top surface as shown in Figure 1. If it is assumed that the shrinkage stress distributes linearly through the thickness of the slab, varying from σ^{sh} at the top to zero at the bottom, the solutions provided by Westergaard (*3*) and Bradbury (*4*) can be implemented only by replacing ϵ' in all of the equations (e.g., Equations 2 to 4) by ϵ^{sh}. Another simplification results in no shrinkage-related stresses within $-H/2 < z < h/2$ ($0 < H < h$, as defined in Figure 1) and that the shrinkage-induced normal stress σ^{sh} linearly decreases from $z = -h/2$ to 0 at $z = -H/2$. Work is under way at the Texas Transportation Institute to model and verify the nonlinear temperature and moisture stress distributions in jointed concrete pavement by numerical analysis techniques.

The following mathematical expressions are provided to lend an adequate explanation for the inclusion of moisture-induced stresses in curling and warping analysis, since analysis of this nature has received little attention in the published literature. The moment caused by the shrinkage-induced, linearly distributed stress when the slab is fully restrained is calculated as follows:

$$M_y^{sh} = -\int_{-\frac{b}{2}}^{-\frac{H}{2}} \frac{\sigma^{sh}}{\frac{h - H}{2}} \left(z + \frac{H}{2}\right) z dz = \tag{10}$$

$$-\frac{\sigma^{sh}}{24(h - H)} \left(2h^3 - 3Hh^2 + \frac{1}{24} H^3\right)$$

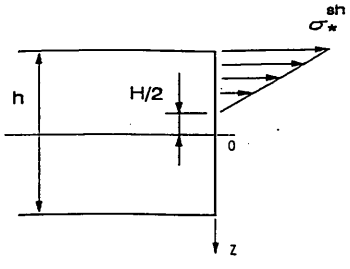

FIGURE 1 Shrinkage-induced stresses.

$$\sigma^{sh} = \frac{E}{1 - \nu} \epsilon^{sh} \tag{11}$$

where ϵ^{sh} is the free shrinkage at the top surface of the pavement, which may be estimated with Equations 6 to 8.

For the warping caused by shrinkage the following equations (in addition to Equation 1) result, corresponding to Westergaard's analysis for the thermal curling case:

$$M_y = D\left[-\frac{d^2w}{dy^2} - \frac{(1 + \nu)(2h^3 - 3Hh + H^3)\epsilon^{sh}}{2(h - H)h^3}\right] \tag{12}$$

$$\frac{d^2M_y}{dy^2} = -kw \tag{13}$$

Therefore, for a slab that has an edge along the x-axis and extends infinitely far in the positive y-axis direction and positive and negative x-axis directions the tensile stress at the top of the slab is

$$\sigma_y = \sigma^{sh}\left[1 - \frac{\sqrt{2}}{4} \frac{(2h^3 - 3Hh^2 + H^3)}{(h - H)h^2} \times \sin\left(\frac{y}{l\sqrt{2}} + \frac{\pi}{4}\right) e^{-\frac{y}{l\sqrt{2}}}\right] \tag{14}$$

$$\sigma_x = \sigma^{sh} + \nu(\sigma_y - \sigma^{sh}) \tag{15}$$

For an infinitely long strip of slab of finite width b with two edges $y = \pm b/2$

$$\sigma_y = \sigma^{sh}\left\{1 - \frac{1}{2} \frac{(2h^3 - 3Hh^2 + H^3)}{(h - H)h^2} \times \frac{\cos\lambda\cosh\lambda}{\sin2\lambda + \sinh2\lambda} \times \left[(\tan\lambda + \tanh\lambda)\cos\frac{y}{l\sqrt{2}} \cosh\frac{y}{l\sqrt{2}} + (\tan\lambda - \tanh\lambda)\sin\frac{y}{l\sqrt{2}} \sinh\frac{y}{l\sqrt{2}}\right]\right\} \tag{16}$$

and σ_x is found from Equation 15.

As seen, the difference between Westergaard's solution and Equation 14 is a factor of the second term in the braces. The numerical solution listed in Tables IV and V in Westergaard's paper can be easily modified for Equation 14. For example, $\sigma_c/\sigma_0 = 1.084$ for $\lambda = b/l\sqrt{8} = 3$ in Table V, but for the shrinkage case with $H = 0$

$$\sigma_y = \sigma^{sh}\left[1 - \frac{\cos\lambda\cosh\lambda}{\sin2\lambda + \sinh2\lambda} (\tan\lambda + \tanh\lambda) \cos\frac{y}{l\sqrt{2}} \frac{\cosh y}{l\sqrt{2}} + (\tan\lambda - \tanh\lambda) \sin\frac{y}{l\sqrt{2}} \sinh\frac{y}{l\sqrt{2}}\right] \tag{17}$$

Comparing Equation 17 with Westergaard's solution results in the following:

$$\frac{\sigma_y}{\sigma^{sh}} = 1 + \frac{(1.084 - 1)}{2} = 1.042$$

Maximum frictional stresses (σ_f) at the midslab area of a concrete pavement may be calculated from the traditional expressions elaborated by Yoder and Witczak (*9*). If the unit weight of concrete is taken as 144 lb/ft^3 then

$$\sigma_f = \frac{L}{2}\mu \tag{18}$$

where μ is the coefficient of subbase friction, and L is the length of the slab. Equation 18 suggests that σ_f will vary directly with L (for a given value of μ); however, a practical limit does exist for σ_f when it equals the maximum frictional stress (σ_m) that results from complete restraint at the bottom of the slab of the climate-induced strains:

$$\sigma_m = E(\epsilon^t + \epsilon^{sh}) \tag{19}$$

Therefore:

$$\frac{L}{2} = L' \leq \frac{1}{\mu} E(\epsilon^t + \epsilon^{sh})$$

where L' represents the length of pavement (from a construction joint) where $\sigma_f = \sigma_m$. Note in Equation 19 that as the friction coefficient increases, the distance to where $\sigma_f = \sigma_m$ decreases.

Friction coefficients depend on the type of subbase and typical coefficients and are listed by others (*10*). The variation in frictional stress along the slab length as it approaches the maximum frictional stress (σ_f) was found to vary nonlinearly by numerical analysis as suggested by McCullough (*10*) and Palmer et al. (*11*). Accordingly, the frictional stress at any point (x) from a construction joint (up to L') of a newly placed pavement may be only linearly approximated by Equation 19 if x is substituted for L' in Equation 19.

Creep Analysis

Creep can generally be defined as a time-dependent deformation of a material subjected to a sustained stress. When deformation is kept constant the creep reduces the stress. This process is defined as relaxation. As suggested by Grzybowski (*12*), stresses that result from relaxation under various strains such as restrained thermal expansion and shrinkage can be calculated by the rate of flow method (*13*). In this method the stress increment $\Delta\sigma_i = \sigma_{i+1} - \sigma_i$ caused by the strain increment $\Delta\epsilon_i = \epsilon_{i+1} - \epsilon_i$ can be obtained as follows:

$$\Delta\sigma_i = \frac{E(t_i)}{1 + \phi(t_{i+1}, t_i)} \Delta\epsilon(t_i) = R(t_{i+1}, t_i)\Delta\epsilon(t_i) \tag{20}$$

where

t = time
$R(t_{i+1}, t_i)$ = relaxation function, and
$\phi(t_{i+1}, t_i)$ = creep coefficient.

From Equation 20 the stress increment $\Delta\sigma_i = \sigma_{i+1} - \sigma_i$ caused by the strain increment $\Delta\epsilon_j = \epsilon_{j+1} - \epsilon_j$, which is imposed at time j before time i, can be calculated as follows:

$$\Delta\sigma = \frac{E(t_j)}{\phi(t_{i+1}, t_i) - \phi(t_i, t_j)} \Delta\epsilon(t_j) \tag{21}$$

The total stress increment that occurs during the ith time interval is the sum of the stress increments $\Delta\sigma_i$ caused by every strain increment $\Delta\epsilon_j (j \leq i)$ and the stress increment caused by the strain increment $\Delta\epsilon_i$:

$$\Delta\sigma_{i,tot} = \sum_{j=1}^{i=1} [R(t_{i+1}, t_j) - R(t_i, t_j)]\, \Delta\epsilon(t_j) + R(t_{i+1}, t_i)\, \Delta\epsilon(t_i) \tag{22}$$

Thus, the stress at the end of the ith time interval can be written as

$$\sigma(t_{i+1}) = \sigma(t_i) + \Delta\sigma_{i,tot} \tag{23}$$

A creep coefficient of the two time instants t and t_0 is suggested in American Concrete Institute (ACI), Standard 209R as

$$\phi(t, t_0) = \frac{(t - t_0)^{0.6}}{10 + (t - t_0)^{0.6}} \phi_\infty(t_0) \tag{24}$$

where

t = actual age of concrete,
t_0 = age of concrete at which the strain increment is imposed, and
$\phi_\infty(t_0)$ = ultimate creep coefficient, depending on the load age, $(t - t_0)$, concrete properties, and environmental conditions.

In the absence of specific creep and shrinkage data for the aggregates and conditions, ACI Standard 209R suggests:

$$\phi_\infty(t_0) = 2.35\, \gamma_c \tag{25}$$

where γ_c is the correction factor, which is the product of correction factors for the load age, ambient relative humidity, the average thickness of the concrete structure, and the cement content, fine aggregate content, and air content in the concrete.

Calculation of Climatic Stresses

The calculation of climatic stresses in a pavement slab at an early age will require the determination of Young's modulus and Poisson's ratio for the concrete. Oluokum et al. (*14*) examined the existing formula for Young's modulus of concrete at an early age proposed by ACI Standard 318. Their investigation showed that the ACI Standard 318 relation for Young's modulus evaluation is essentially valid at concrete ages 12 hr and greater:

$$E = 57{,}000\sqrt{f'_c} \tag{26}$$

where f'_c is compressive strength of concrete (in psi).

Klink (*15*) and Higginson (*16*) observed that Poisson's ratio of concrete varied little at different ages and curing conditions. According to their observations Poisson's ratio is insensitive to the mixture content as well as age and it may be taken as 0.15.

For discussion purposes the climatic stresses in a 13-in. concrete slab constructed in Texarkana, Tex., placed directly on subgrade were calculated. It was assumed that the test pavement,

during the period of crack development, behaved as an infinitely long slab of finite width b (assuming a 24-ft-wide, two-lane pavement). The frictional subbase stresses (σ_f) are calculated according to Equation 18 on the portion of the pavement segment where curling and warping stresses are a maximum. This was shown by Westergaard to be 4.44l from a free edge (the construction joint for new pavements) or greater. The computation of frictional stresses is based on the temperature and moisture changes that occur at the bottom of the slab and the appropriate coefficient of friction for an untreated clay subgrade (μ = 1.5).

Information from one of the concrete mix designs used in experimental pavement sections referred to previously is used in demonstrating the development of early-age stresses in jointed concrete pavements. The following data show the mix design ratios relevant to Equation 6: a/c = 7.36, w/c = 0.51, g/s = 1.36, and s/c = 2.80.

For this mix design the correction factor relevant to the equation for relaxation analysis is the product of all of the correction factors listed in Table 1.

Field data collected during the first 5 days after construction and placement of the concrete consisted of the slab temperature and the humidity profile. From these data the history of the maximum stresses in the slab was determined over the 5-day period; however, the history is not illustrated here because of space requirements. Maximum curling (σ^t) and warping (σ^{sh}) stresses over the first few days of construction require the determination of the time-dependent properties (compressive strength, modulus of elasticity, and l-value) of the concrete that vary during and for a period of time after hardening. The variation in the compressive strength (f'_c) of the concrete is shown in Figure 2. Noting how these parameters vary with time, it is no surprise to see a variation in the maximum σ^t and σ^{sh} values (as determined at the surface in the longitudinal direction). Since the pavement under consideration was placed directly on subgrade, the subgrade k-value was taken as 100 psi/in. Frictional stresses are calculated, as pointed out previously, on the basis of the temperature and moisture changes at the slab bottom; depending on the magnitude and direction of change, the total stresses may be tensile or compressive. The shrinkage stresses were calculated by using Equations 6 to 8 and the ratios tabulated previously. Equation 16 yields the warping stresses in the longitudinal direction. The warping stresses in the longitudinal direction include σ^{sh} (= σ_0 in this case) because of a shrinkage-caused gradient. The Bradbury expressions (Equations 3 and 4) are used to find similar thermal stresses. The combination of or total stresses discussed above were determined at a distance of 90 ft from the pavement end. The stresses were found at this distance because this is approximately where maximum restraint occurred in the paved segment, which approaches the center of the paved segment.

The sum of the combination of curling, warping, and friction will vary along the longitudinal axis of the paved segment. The maximum combination of these stresses, which occurs near the center of any paved segment, may be dominated by the frictional component. However, curling and warping stresses may dominate near the free edge of the paved segment. By considering the process of relaxation, the resultant of these two stress components is calculated by using Equations 20 to 25. The maximum friction-caused stress at 90 ft from the pavement free edge (where a first crack was found near the center of the paved segment) is 141 psi for a pavement thickness of 12 in., a unit weight of concrete of 150 lb/ft^3, and a friction coefficient of 1.5. The total longitudinal stress at the top of the pavement is the sum of the curling, warping, and friction-caused stresses at that location. Figure 3 shows the superposition of these three stresses at 90 ft from the pavement free edge. The dashed line includes only the combination of the curling and warping stresses. When the contribution caused by curling and warping is less than 141 psi the subbase friction dominates the restraint to slab movement and causes stresses that are equal to the value of the combination or exceeds them. The bold solid line in Figure 3 is the result of the superposition, the total longitudinal stress at the top of the pavement (which includes creep). Cracking appears to occur initially in the portion of the paved segment of maximum restraint and then proceeds from this point at intervals of 4.44l.

SAWCUT SPACING DEPTH REQUIREMENTS

To determine the spacing of the transverse joint locations or sawcuts for a newly placed concrete pavement for the purpose of stress analysis, the assumption that a newly paved pavement is infinitely long applies. Therefore, the maximum total climatic stress (as described previously) is calculated at approximate intervals of 4.44l as predicted by Westergaard analysis. The position of maximum stress may vary for early-age concrete because l changes during this period of time. As the concrete ages, maximum stress locations typically stabilize at 13- to 16-ft intervals, depending on the subbase type, which provides some guidance as to the recommended joint spacing for design and construction purposes.

The same analysis may apply to the spacing of the longitudinal sawcut locations; however, the focus in this instance is normally examination of the suitability of using standard joint locations, which often serve as lane dividers. In a two-lane pavement the longitudinal tensile stress at the pavement top is calculated at the longitudinal joint location (such as along the center line, where the pavement is divided into two 12-ft-wide strips) and the total tensile stress σ_x is reduced by a factor of 50 percent according to

TABLE 1 Correction Factors for Ultimate Creep Coefficient

variable	load age $(t-t_0)$	ambient R.H.=75%	pavement thickness h=12in	Slump s=1.5in	Cement Content c=521 lb/yard^3	air content α=5%	fine aggregate percentage ψ=35.9%
Correction factor	$1.25(t-t_0)^{-0.118}$	0.768	0.864	0.92	0.938	1	0.966

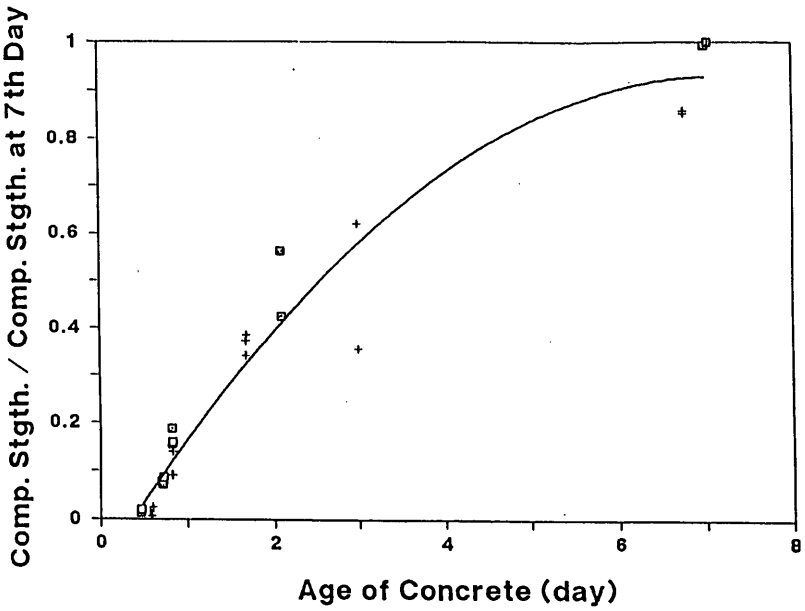

FIGURE 2 Variation in compressive strength of early-age concrete.

Equation 16, which in this case is below the tensile strength of concrete.

THEORY AND APPLICATION OF FRACTURE MECHANICS

The analysis of a notched concrete pavement slab on the basis of fracture mechanics incorporates the stresses generated by temperature and shrinkage effects, which are applied as loads. Important material parameters identified by the Size Effect Law (*17*) are determined on the basis of notched beam tests. The notch depth is great enough such that the crack will develop quickly and extend to the slab bottom under the applied stress. Through fracture tests the fracture parameters K_{If} and C_f have been obtained for early-age concretes made up of different coarse aggregates (*18*). The K_{If} is the critical stress intensity factor for a specimen of infinite dimension (in depth), in which linear elastic fracture mechanics (LEFM) applies to the analysis thereof. With respect to the application of K_{If} to a concrete slab, LEFM can still be applied to determine a sufficient notch depth, even though a concrete slab is not infinitely large. This is because the nominal strength of a specimen of infinite dimension is lower than the nominal strength that is predicted for the specimen of finite dimension by LEFM on the basis of K_{If} as the failure criterion.

As in linear mechanics the superposition principle can be used for the stress intensity when a specimen or structure is subjected to more than one load. The stress intensity factor caused by any load can always be expressed as follows:

$$K_I = \sigma \sqrt{\pi a}\, N(\omega) \tag{27}$$

where

σ = nominal stress,
a = crack length, and
$N(\omega)$ = nondimensional function of the ratio, ω, of the crack length a to the specimen dimension d.

$N(\omega)$ is called the nominal stress intensity factor. The beam depth (pavement thickness h) is usually taken as the dimension d. $N(\omega)$ is dependent on the specimen geometry but is independent of the specimen size. The nominal stress intensity factor $N(\omega)$ for the simple tension (*19*) is

$$N(\omega) = 1.122 - 0.231\omega + 10.550\omega^2 - 21.710\omega^3 + 30.382\omega^4 \tag{28}$$

where $\omega = a/h$ [Figure 4(*a*)] and the nominal stress σ is the load intensity. For the pure bending (*19*)

$$N(\omega) = 1.122 - 1.40\omega + 7.33\omega^2 - 13.08\omega^3 + 14.0\omega^4 \tag{29}$$

where $\omega = a/h$ [Figure 4(*b*)] and the nominal stress σ is the maximum stress in the distributed load. Note that these two formulas are for the geometry with top and bottom surfaces free from external forces. Because of the tendencies of curling and warping caused by the temperature gradient and shrinkage, Equation 29 is approximately valid. A double edge notched test specimen can be used to develop the fracture analysis because this specimen is somewhat representative of a slab configuration since the centerline in this symmetrical specimen is assumed not to move in the vertical direction. The following equation is valid for $\omega = (a/h) < 0.7$:

$$N(\omega) = 1.12 + 0.203\omega - 1.197\omega^2 + 1.930\omega^3 \tag{30}$$

where the nominal stress σ is the load intensity. Equations 8 and 9 are useful in applying the stress field induced by climatic effects to the determination of the stress intensity given in Equation 27

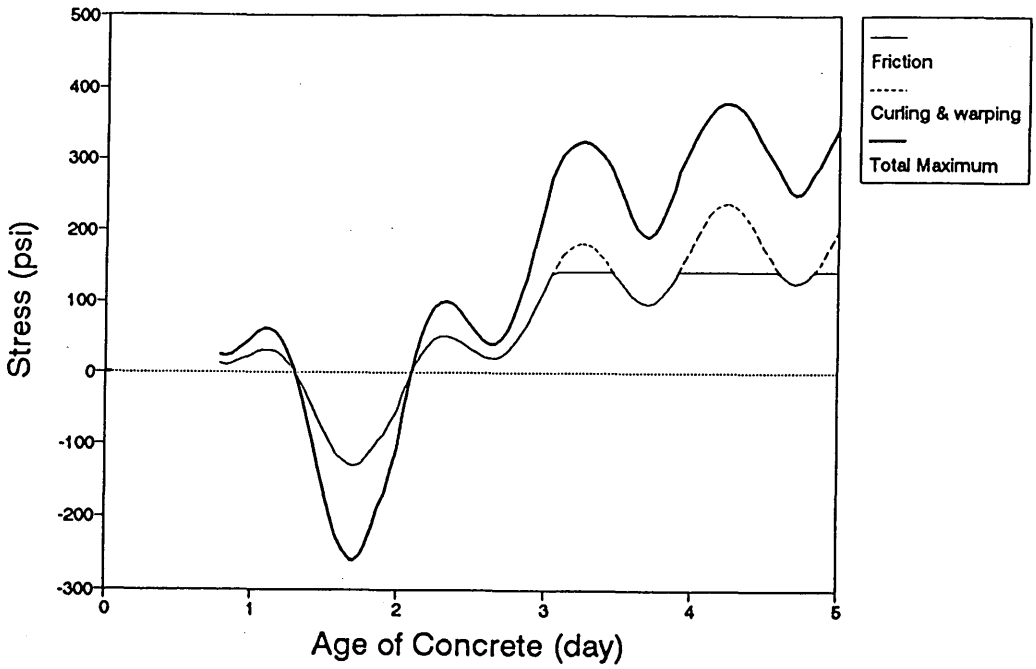

FIGURE 3 Development of stress at concrete pavement surface.

by dividing the stress field into components of tensile forces and bending moments. The finite-element analysis in this study has shown that replacement of the distributed load on a specimen by its resultant does not yield significant change in the K_I value, particularly when the specimen length is four times the thickness. Equation 29 can be applied to pure bending loads other than that shown in Figure 4(*b*) by substituting $\sigma = 6M/h^2$. Equation 30 can be applied to tensile loads on a single edge notched specimen whose unnotched edge remains straight. Accordingly, the shrinkage-induced stresses are transformed to a tensile force and a bending moment. For instance, if $H = h/2$, the resultant tensile force is $h\,\sigma^{sh}/8$, and then Equation 30 can be used in Equation 27 by substituting $\sigma = \sigma^{sh}/8$ (the resultant force). The bending moment $M = (5/96)\,\sigma^{sh}h^2$ yields $\sigma = (5/16)\,\sigma^{sh}$, in which case Equation 29 can be used. K_I results from the sum of Equations 29 and 30.

Determination of the stress intensity given in Equation 27 can be accomplished for a given set of climatic conditions at the anticipated sawcut location to generate the sawcut depth guidelines shown in Figure 5. The K_I values with different notch (sawcut) depths under temperature and shrinkage stresses are determined by Equations 29 and 30. Figure 5 also gives the K_I values for temperature differences t of 10, 20, 40, and 50°F between the pavement top and bottom with the same shrinkage-induced stresses.

The type of coarse aggregate is also important. When the critical stress intensity factor K_{If} equals or exceeds the fracture tough-

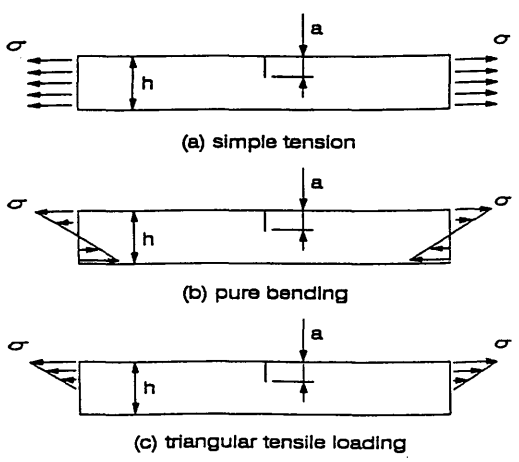

FIGURE 4 Notched specimens under loading.

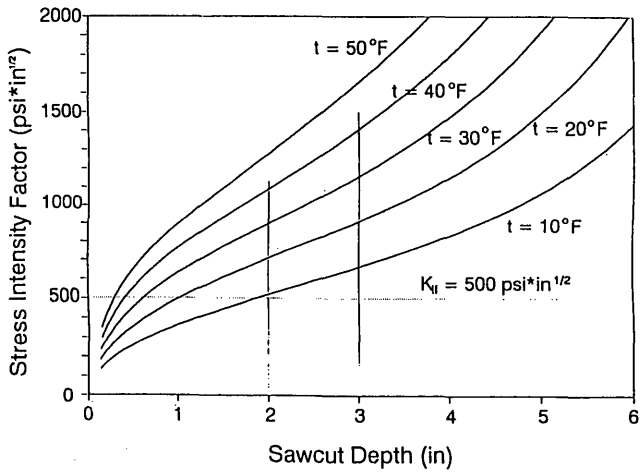

FIGURE 5 Determination of sawcut depths.

ness, K_{If} = 500 psi $\sqrt{\text{in.}}$ (typical for river gravel concrete at an age of 12 hr), a sawcut depth of 1 in. is enough if the temperature difference is not less than 20°F. When K_{If} = 800 psi $\sqrt{\text{in.}}$ (typical for limestone concrete at an age of 12 hr), a sawcut depth of 1.7 in. is enough if the temperature difference is not less than 30°F. Noting the change in stress intensity in comparison with the fracture toughness for the given climatic conditions, one can develop a sense for the appropriate sawcut timing to control cracking at the sawcut notches.

FIELD INVESTIGATION OF CRACK CONTROL

As pointed out previously, the factors that affect the behavior of concrete pavement as they relate to joint formation and crack control were monitored in a field study undertaken at test sections in Texarkana, Tex., for a 13-in. jointed plain concrete pavement placed directly on subgrade soils. Several factors were considered in these test sections such as different types of coarse aggregate, different curing methods, and different sawcut techniques and are elaborated further elsewhere (*9,20*) along with the type of concrete mixtures that were placed on subgrade soils. These mixtures consisted of different coarse aggregate types and blends. However, some results of the crack survey for the observation of joint and crack formation are provided here and coincide with the calculations given previously. Ambient and pavement temperatures and relative humidities were measured as indicated previously. The development of K_I and K_{If} is calculated and is shown in Figure 6. This analysis suggests that cracking initiated 4 to 5 days after placement.

The joints in the test section pavement in Texarkana were sawcut by two different techniques at 15-ft intervals. One method consisted of conventional sawcut techniques that used water to cool the saw blade. By this technique the pavement was cut 3-in. deep ($d/4$). The other method consisted of early-age sawcut techniques. By this technique a light and portable sawcutting machine was used so that a pavement surface notch could be placed early in the pavement life (typically less than 2 to 3 hr after placement). This was achieved without noticeable joint raveling. Typical sawcut depths were 1 in., and no cooling water was used in the process. Crack surveys conducted from October 1991 to July 1992 indicated that of all the transverse cracks that developed, only two occurred in between the sawcut joints. These two uncontrolled cracks were initiated from the corners of blockouts (i.e., inlet drainage structures), where stress concentration would have existed. It is speculated that these stress concentrations at the sharp corners could be avoided by placing joint locations so that they coincided with any sharp corners to guide cracking such that uncontrolled transverse cracks would not occur.

Although the pavement test section in Texarkana was paved on November 8, 1991, no visible cracks were found until November 26, 1991. Cracks at the sawcut tip were observed through the bottom of the pavement slab in later surveys. Earlier cracks occurred at a distance from the pavement construction joint since sufficient stresses needed to develop because of pavement restraint. It should be noted that on June 4, 1991, more joints had been formed at the early-age sawcuts than at the conventional sawcuts. One month later, three more cracks were found at the conventional sawcuts. A significant amount of cracking developed after the pavement was subjected to a greater temperature cycle range. Since the strength of the concrete increased prior to the increase in cracking, it is speculated that cracking at the sawcuts, although observed much later after construction, initiated early in the life of the pavement, which may be indicative of the fact that a certain level of damage is necessary to ensure that cracking will occur at the sawcut joint.

A closer look at the evolution of cracking indicated that the initial crack interval was on the order of 90 ft or more. Apparently, it is intervals of this magnitude at which the combination of curl, warping, and frictional stresses was enough to initiate cracking (Figure 6). The frictional stress may have been the significant contributor to crack development given the climatic conditions under

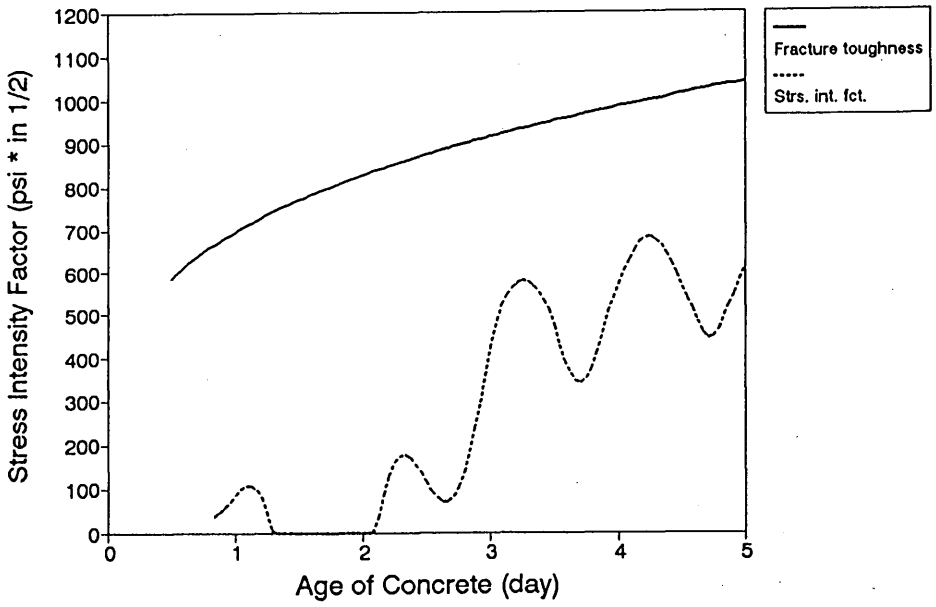

FIGURE 6 Development of stress intensity and fracture toughness.

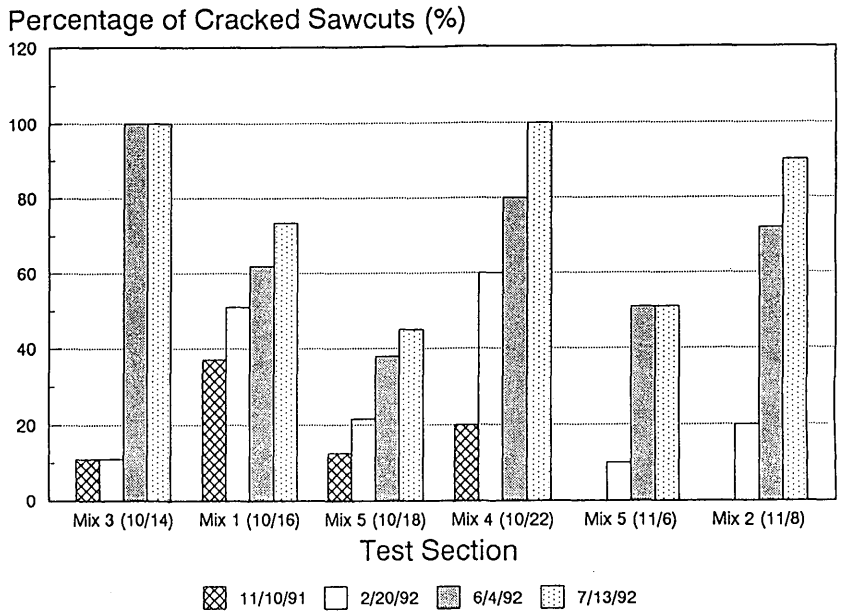

FIGURE 7 Percentage of sawcuts with cracks observed at different dates in test sections paved at different dates (in parentheses) with different concrete mix designs.

which the paving was accomplished, although a much improved crack pattern developed the following summer. The disadvantage of a crack pattern developing in this manner is that some joints open wider than they were designed to, which may damage the joint sealant material. It should be pointed out this characteristic was prevalent whether conventional or early-age cutting techniques were used. This situation deserves further consideration in future cracking studies.

It is interesting to note that different types of aggregate affect the fracture properties and crack development of concrete pavement, as shown in Figure 7. Cracking at the sawcut tip occurred more frequently when the concrete coarse aggregate type was river gravel than when it was crushed limestone. This was also the case in the subsection paved with the concrete that used a blend of crushed limestone and river gravel as the coarse aggregate in comparison with that in the subsection paved with the concrete that used crushed limestone only as the coarse aggregate. Laboratory tests showed that concrete of crushed limestone had a higher fracture strength than that of concrete of river gravel at early ages (*10,18*). These field results tend to confirm the validity of using early-age sawcutting techniques. Although not expressly addressed in this paper, it appears that sawcut timing is much more significant than sawcut depth. A shallow notch placed early in the pavement surface can take advantage of the greater change in temperature and moisture in the vicinity of the pavement surface (in comparison with the changes at a greater depth), which results in a greater amount of crack damage and subsequent incidence of cracking at the shallow surface notches.

CONCLUSIONS

Modified linear fracture mechanics is applicable for determining sawcut depth for cracks that develop early. The sawcut depth is dependent on the spacing of the transverse sawcut, the material fracture parameters K_{If} and C_f, and the stress level in the concrete slab with given geometrical conditions. The material fracture parameters vary with time, especially at early ages of concrete. Field observations have found that late-appearing cracks are also initiated by shallow (1 in.) sawcut notches. However, the propagation of these cracks may be caused by long-term fluctuating thermal and moisture loads, for which further research is needed.

The reduction of the sawcut depth (less than $d/3$ or $d/4$) at concrete joints by early-age sawcut or placement techniques can take advantage of the greater change in moisture and temperature in the concrete at the pavement surface (in comparison with the change at $d/3$ or $d/4$) to initiate a greater incidence of cracking at the notches than would otherwise be the case. Therefore, the control of cracking of concrete pavement should be improved. Field surveys indicate that under some circumstances (such as paving under cool weather conditions) transverse cracks at the sawcut notches may initiate much later after placement. On a preliminary basis this study indicates that it is reasonable to use notch depths at an early concrete age on the order of 1 in. to initiate cracking at the pavement surface, which is significantly less than the traditional $d/4$ or $d/3$.

ACKNOWLEDGMENTS

Appreciation is extended to the Texas Department of Transportation and FHWA for financial support under Project 1244. This paper is based on portions of the results of the study.

REFERENCES

1. Emborg, M. *Thermal Stresses in Concrete Structures at Early Ages.* Doctoral thesis. Luleå University of Technology, Luleå, Germany, 1989.

2. Richardson, J. M., and J. M. Armaghani. Stress Caused by Temperature Gradient in Portland Cement Concrete Pavements. In *Transportation Research Record 1121*, TRB, National Research Council, Washington, D.C., 1987.
3. Westergaard, H. M. Analysis of Stresses in Concrete Pavements Due to Variations of Temperature. *HRB*, Vol. 7, HRB, National Research Council, Washington, D.C., 1927.
4. Bradbury, R. D. *Reinforced Concrete Pavements*. Wire Reinforcement Institute, Washington, D.C., 1938.
5. Tang, T., D. G. Zollinger, and S. Senadheera. Analysis of Concrete Curling in Concrete Slabs. *Journal of Transportation Engineering*, July/September 1993, pp. 618–633.
6. Bažant, Z. P., and S. T. Wu. Creep and Shrinkage Law for Concrete at Variable Humidity. *Journal of the Engineering Mechanics Division*, Vol. 100, 1974.
7. Bažant, Z. P., and L. Panula. Practical Prediction of Time-Dependent Deformation of Concrete. Part 3: Drying Creep. Part 4: Temperature Effect on Basic Creep. *Matériaux et Constructions*, Vol. 11, No. 66, 1978.
8. Buch, N., and D. G. Zollinger. Preliminary Investigation on the Effect of Moisture on Concrete Pavement Strength and Behavior. In *Transportation Research Record 1382*, TRB, National Research Council, Washington, D.C., 1993.
9. Yoder, E. J., and M. W. Witczak. *Principles of Pavement Design*, 2nd ed. John Wiley & Sons, Inc., New York, 1975.
10. McCullough, B. F. *Mechanistic Analysis of Continuously Reinforced Concrete Pavements Considering Material Characteristics, Variability, and Fatigue*. Research Report 1169-2. Center for Transportation Research, University of Texas at Austin, April 1990.
11. Palmer, R. P., M. Olsen, and R. L. Lytton. *TTICRCP—A Mechanistic Model for the Prediction of Stresses, Strains, and Displacements in Continuously Reinforced Concrete Pavements*. Research Report 371-2F. Texas Transportation Institute, Texas A&M University, College Station, Aug. 1987.
12. Grzybowski, M. *Determination of Crack Arresting Properties of Fiber Reinforced Cementitious Composites*. Royal Institute of Technology, Stockholm, Sweden, 1989.
13. England, G. L., and J. M. Illston. Methods of Computing Stress in Concrete from a History of Measured Strain. *Civil Engineering and Public Works Review*, Vol. 60, No. 705, No. 706, and No. 707, 1965.
14. Oluokum, F. A., E. G. Burdette, and J. H. Deatherage. Elastic Modulus, Poisson's Ratio, and Compressive Strength Relationship at Early Ages. *ACI Material Journal*, Vol. 88, No. 1, 1991.
15. Klink, S. A. Aggregates, Elastic Modulus, and Poisson's Ratio of Concrete. *ACI Journal, Proceedings*, Vol. 83, No. 6, Nov.–Dec. 1985.
16. Higginson, I. L. Effect of Steam Curing on the Important Properties of Concrete,'' *ACI Journal, Proceedings*, Vol. 58, No. 3, 1961.
17. Bazant, Z. P., and M. T. Kazemi. Determination of Fracture Energy Process Zone Length and Brittle Number from Size Effect, with Application to Rock and Concrete. *International Journal of Fracture*, Vol. 44, 1990.
18. Zollinger, D. G., T. Tang, and R. H. Yoo. Fracture Toughness of Concrete at Early Ages. *ACI Material Journal*, Vol. 90, No. 5, Sept.–Oct. 1993.
19. Tada, H., P. C. Paris, and G. R. Irwin. *The Stress Analysis of Cracks Handbook*. Paris Productions Inc., St. Louis, Mo., 1985.
20. Tang, T., D. G. Zollinger, and F. McCullough. *Concrete Pavement Field Tests in Texarkana and La Porte*. Research Report 1244-7. Texas Transportation Institute, Texas A&M University, June 1994.

Publication of this paper sponsored by Committee on Rigid Pavement Design.